Journal of Theoretical and Applied Mechanics, Sofia, Vol.52 (2022) pp. 365-380
SOLID MECHANICS

INFLUENCE OF TYPE OF ADHESIVE ON THE INTERFACE DEBONDING OF A $BaTiO_3$/EPOXY STRUCTURE UNDER TIME HARMONIC MECHANICAL LOAD AND ELECTRIC FIELD AT ENVIRONMENTAL CONDITIONS

TATYANA PETROVA[1], ELISAVETA KIRILOVA[1*],
WILFRIED BECKER[2], JORDANKA IVANOVA[3]

[1]*Bulgarian Academy of Sciences, Institute of Chemical Engineering,*
Acad. G. Bonchev Str., bl. 103, 1113 Sofia, Bulgaria
[2]*Technical University of Darmstadt,*
Franziska-Braun-Straße 7, 64287 Darmstadt, Germany
[3]*European Polytechnical University,*
23 Sv. Sv. Kiril i Metodiy Str., 2300 Pernik, Bulgaria

[Received: 26 February 2022. Accepted: 05 April 2022]

doi: https://doi.org/10.55787/jtams.22.52.4.365

ABSTRACT: The study deals with investigation of the effect of the used adhesive upon the interface delamination at adhesively bonded piezoelectric patch/layer structure $BaTiO_3$/Epoxy subjected to time harmonic mechanical load and electric field at environmental conditions. This is needed for a prediction of conditions, at which these type of structures work safely (without failure). For the interface shear stress in the overlap zone of structure, at two different thicknesses of its adherends and three adhesives used, a solution method based on shear lag and Fourier method has been applied. The types of solutions obtained depend mainly on the adherends' thickness, the magnitude and frequency of the applied mechanical loading and the shear modulus of the used adhesive. Based on the analysis conducted it has been shown that with increasing magnitude and frequency of applied mechanical load, the delamination length also increased. The delamination could be avoided if the stronger adhesives and thicker adherends are chosen. The debond length is highly dependent on the magnitude of electric displacement. The analytical equation for resonant frequencies in the considered structure is developed on the base of obtained solutions and they are calculated at all three investigated adhesives.

KEY WORDS: patch/layer structure; adhesive influence; interface debonding; dynamic time harmonic mechanical and electric load.

*Corresponding author e-mail: e.kirilova@iche.bas.bg

1 INTRODUCTION

Over the last decades, the damage tolerance design of adhesive bonded joints has become significantly important in the aerospace industry as well as automotive, marine and other industries. The design parameters which affect the strength and durability of adhesive bonded joints are surface treatment; joint configuration; geometric and material properties of adhesive layer and adherends; the type of applied loading and environmental conditions [1]. The type of bonding method [2] and the critical strain field [3] also affect the strength of the considered adhesive bonded joints. These parameters are very important when the stress strain behavior of the smart patch/layer structure is considered [4]. For damage tolerance design of such type of structures it is very useful to predict the stress distribution and the conditions, at which adhesive bonded joints work safely (without failure) under a given loading (static or dynamic). For that purpose, closed-form analytical methods and numerical methods such as finite element method (FEM), boundary element method and finite difference methods have been developed [5, 6].

FEM are used mainly for investigation of the fracture behavior and geometric and mechanical properties of adhesive layer and bonding conditions. For example, Zhu and Kedward [7] have investigated by FEM and closed-form solutions the thickness and ductility of the adhesive layer in adhesively bonded joints under tensile shear loading for stress distribution and failure prediction. Based on the analysis conducted it has been shown that the maximal strength of the adhesively bonded single lap joint increased with decreasing adhesive thickness. Matt et al. [8] have investigated the behavior of composite adhesively bonded joints at the presence of bond defects by a semi-analytical FEM and experimentally by ultrasonic testing the propagation of ultrasonic guided waves across the joints with poorly cured adhesive and disbonded interfaces. The obtained results have shown that the ultrasonic energy transmission through the joint is highly dependent on the bond conditions, with defected bonds resulting in increased transmission strength. Sandu et al. [9] have evaluated the load capacity of some configurations of adhesively bonded single-strapped joints based on analytical pre-dimensioning calculus and nonlinear elastic finite element analysis. The authors have discussed that a spectacular improvement of strength performance of single strapped-joints with small gaps between the adherends ends can be obtained by filling the gap with adhesive and by using straps thicker than the outer adherends. Tinoco et al. [10] have conducted a numerical FEM analysis to understand adhesive layer effects on the electromechanical coupling of piezoelectric sensors bonded to the structures. The authors have developed a mathematical model for electrical signatures using Maxwell's equation (Gauss law for electricity). The obtained results have shown that the thickness and the length of the adhesive layer have significant

effects on the electrical signatures and these effects can be applied to detect debonding of piezoelectric sensors. Afendi et al. [11] have used finite element analysis for investigation of the effect of bond thickness upon the shear strength of an epoxy adhesively bonded joint with dissimilar adherends. The obtained results have shown that the shear strength of the adhesive joint decreases with increasing bond thickness and the strength of the shear adhesive joint is also dependent on the elastic modulus of the adherend. Some authors incorporated cohesive zone models in finite element analysis for prediction of the repair's elastic stiffness, maximum load and corresponding displacement in the bonded assemblies [12] as well as for prediction of failure initiation and delamination pattern of such adhesive joints [13].

Besides FEM, other methods for analysis of the stresses in bi-material adhesive bonded structures have been developed. For example, Chadegani and Batra [14] have used first-order shear deformation plate theory for the case of a void within the adhesive of such type of structures. For each section the authors have formulated balances for forces and moments and the continuity of displacements as forces and moments at the interfaces between the adjoining sections has been imposed. On the other hand, Valeva et al. [15] have used 2D boundary element method to determine the debond length along the interface in a pre-cracked bi-material ceramic-metal structure. Jin and Wang [16] have proposed a sensor model for investigation of the effect of mechanical and geometrical properties of the adhesive layer on the coupled dynamic electromechanical behavior of a thin piezoceramic sensor bonded to an elastic medium.

Furthermore, the behavior of bonded joint structures is affected by the properties of the adhesive used. Hass et al. [17] have studied the failure of adhesive bondlines at microscopic level via tensile test and the interaction of cracks with adhesive bondlines under various angles to the crack propagation as well as the respective loading situations for the adhesives: urea-formaldehyde (UF), polyurethane (PUR) and polyvinyl acetate (PVAc) which have distinctly different mechanical behaviors. Fernandes et al. [18] have investigated experimentally and numerically by finite element analysis, cohesive zone models (CZM) and extended finite element method (XFEM) the performance of three polyurethane adhesives ranging from brittle to largely ductile behavior in single lap joints with varying values of overlap length. They have evaluated which family of adhesives is more suited for a given joint geometry.

The proved performance of the shear lag method in the case of combined dynamic time harmonic load, electric field at environmental conditions of smart hygropiezothermal elastic patch/layer configurations has encouraged us to apply it for the investigation of the magnitude and the frequency of applied mechanical load as well as the electric displacement at which a possible interface delamination appears [19]. The efficiency of the proposed approach in [19] is proved on a adhesively

bonded patch/layer structure PZT-5H/CFRP with polyacrylate thermoplastic adhesive. Three type of closed-form solutions are obtained for the interface shear stress in the structure. The results show that the choice of the ratio of of the thicknesses of the patch and the host layer plays a significant role on the interface shear stress and debond length. Decreasing ratio of the thicknesses of the adherends leads to an enlargement of the frequency interval at which no delamination appears. On the other hand, the frequency interval of applied dynamic load can change drastically the type of the solution at given constant ratio of thicknesses of the adherends.

The current work continues our investigations in [19], adding an additional factor affecting the debonding in bonded patch/layer structures under the applied dynamic time harmonic load and electric field at environmental conditions – the type of the adhesive used. Three types of adhesives are considered and their influence on both the interface shear stress and the debond length is represented at case study of $BaTiO_3$/Epoxy structure, subjected on the applied dynamic time harmonic load and electric field at environmental conditions. Shear-lag model predictions [19] for interface shear stress and debond length are illustrated for each of the adhesives considered, for two type of solutions with the same thickness ratio for the structure adherends, but at different thickness of layers. The influence of the electric displacement and the magnitude of the mechanical load and frequency on the delamination in the considered patch/layer structure are also investigated.

2 Model Solutions

The detailed description of solution derivation is given in [19] and here for brevity only the final differential equations for the displacements u_A and u_B in the structure layers A and B (Fig. 1), boundary conditions (BC) and solutions for interface shear stress τ_I, deformation u'_A in layer A and electric gradient E_{zA} are presented:

$$u''_A - k(u_A - u_B) = -\xi u_A\,, \quad u''_B + \lambda(u_A - u_B) = -\eta u_B\,, \tag{1}$$

$$u'_A(0) = 0\,, \quad u'_A(l) = 0\,, \quad u'_B(0) = \sigma_0\,, \quad u'_B(l) = \sigma_0, \tag{2}$$

where the following notations are introduced for simplicity:

$$E_A = c_{11}^{A*} + \frac{e_{13}^{A*} e_{31}^{A*}}{\varepsilon_{33}^{A*}}\,; \quad E_B = c_{11}^{B*}\,; \quad D_A = \frac{e_{13}^{A*}}{\varepsilon_{33}^{A*}} D_0\,;$$

$$\xi = \frac{\rho_A}{E_A}\omega^2\,; \quad \eta = \frac{\rho_B}{E_B}\omega^2\,; \quad k = \frac{1}{h_I h_A}\frac{G_I}{E_A}\,; \quad \lambda = \frac{1}{h_B h_I}\frac{G_I}{E_B}\,;$$

$$\alpha_A = \left(\alpha_{11}^{A*} - \frac{e_{13}^{A*}}{\varepsilon_{33}^{A*}} p_3^{A*}\right)\,; \quad \alpha_B = \alpha_{11}^{B*}\,; \beta_B = \beta_{11}^{B*}\,; \tag{3}$$

$$\tau_I = G_I \frac{(u_A - u_B)}{h_I}\,; \quad E_{zA} = \frac{D_{zA}}{\varepsilon_{33}^{A*}} - \frac{e_{31}^{A*}}{\varepsilon_{33}^{A*}}\varepsilon_A - \frac{p_3^{A*}}{\varepsilon_{33}^{A*}} T\,; \quad h_I = h_A + h_B,$$

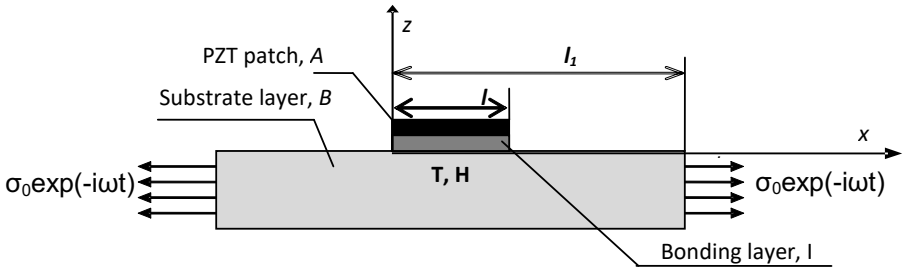

Fig. 1: The model of the smart patch/layer structure.

where h_A, h_B are the thicknesses of the adherends, c^*_{ij}, $(i,j = 1 \div 3)$ are the elastic constants transformed from 3D case to 1D case (measured at constant electric field), e^*_{ij} and ε^*_{ij} are piezoelectric and dielectric constants (measured at constant strain), α^{A*}_{11}, β^{A*}_{11}, α^{B*}_{11}, β^{B*}_{11} are thermal and hygromechanical stress coefficients for the respective adherends, p^{A*}_3 is the pyroelectric coefficient for the patch A, α_k, β_k are thermal and moisture expansion coefficients for the layers, E_k, is Young's modulus for the layers $(k = A,\ B)$ and G_I is the shear modulus of the interface layer I, respectively. E_{zA}, D_{zA} are the electric gradient and the electric displacement of the patch. The poling axis is along the axis 0z, the origin of Oxz is set at the left end of the overlap zone. The problem is solved in the selected overlap zone $0 < x < l$ with length l (Fig. 1) for the lightweight structure of the smart patch and hosting layer, where is assumed that $D_{zA} = D_0 = \text{const}$.

After some transformations of Eqs. (1), we get the following differential equation for the patch displacement:

$$(4)\quad u^{IV}_A - AAu''_A - BBu_A = 0, \quad AA = k - \xi + \lambda - \eta, \quad BB = k\eta - \xi\eta + \lambda\xi\,.$$

The corresponding characteristic equation is: $r^4 - AAr^2 - BB = 0$, $r^2 = z$, $z^2 - AAz - BB = 0$ with the roots $z_{1,2} = \left(AA \pm \sqrt{AA^2 + 4BB}\right)/2$.

The following solutions of Eq. (4) for the displacements u_A and u_B, the electric gradient E_{zA} and the shear stress τ_I are given for 3 cases (two positive, one positive and one negative, and two negative roots of the characteristic equation for z in Eq. (4)). The type of roots depends mostly (see the parameters in Eq. (3)) on the material properties of the layers, their thickness, the applied frequency, and the shear modulus of the adhesive used. Related to the materials chosen in the next section, here only solutions for CASE 2 and CASE 3 for interface shear stress, deformation and electric gradient in piezo-electric layer A will be presented.

CASE 2 : ONE POSITIVE AND ONE NEGATIVE ROOT $z_1 > 0$, $z_2 < 0$ WITH

$$
\begin{aligned}
r_1 &= \pm\sqrt{z_1}\,, \quad r_2 = \pm i\sqrt{|z_2|}\,,\\
\tau_I(x) &= \frac{G_I}{h_I k}\Big\{(\xi + r_1^2)[A_1\cosh(r_1 x) + A_2\sinh(r_1 x)]\\
&\quad + (\xi - r_2^2)[A_3\cos(r_2 x) + A_4\sin(r_2 x)]\Big\},\\
u'_A(x) &= r_1 A_1\sinh(r_1 x) + r_1 A_2\cosh(r_1 x)\\
&\quad - r_2 A_3\sin(r_2 x) + r_2 A_4\cos(r_2 x)\,,\\
E_{zA} &= \frac{D_0}{\varepsilon_{33}^{A*}} - \frac{e_{31}^{A*}}{\varepsilon_{33}^{A*}}u'_A - \frac{p_3^{A*}}{\varepsilon_{33}^{A*}}T\,.
\end{aligned}
\tag{5}
$$

The integration constants A_i, $i = 1 \div 4$, are obtained from the boundary conditions Eq. (2) and are

$$
A_1 = -\frac{[b - a(k - \xi + r_2^2)][1 - \cosh(r_1 l)]}{r_1(r_1^2 + r_2^2)\sinh(r_1 l)}\,, \qquad A_2 = -\frac{[b - a(k - \xi + r_2^2)]}{r_1(r_1^2 + r_2^2)}\,,
$$

$$
A_3 = \frac{[b - a(k - \xi - r_1^2)][\cos(r_2 l) - 1]}{r_2(r_1^2 + r_2^2)\sin(r_2 l)}\,, \qquad A_4 = \frac{[b - a(k - \xi - r_1^2)]}{r_2(r_1^2 + r_2^2)}\,.
$$

The following equal notations

$$
a = \frac{D_A + \alpha_A T}{E_A}\,, \quad b = \frac{\sigma_0 + \alpha_B T + \beta_B H}{E_B}
$$

are used for both CASE 2 and CASE 3 in integration constants A_i for brevity.

CASE 3 : TWO NEGATIVE ROOTS $z_1 < 0$, $z_2 < 0$ WITH

$$
\begin{aligned}
r_1 &= \pm\, i\sqrt{|z_1|}\,, \quad r_2 = \pm i\sqrt{|z_2|}\,,\\
\tau_I(x) &= \frac{G_I}{h_I k}\Big\{(\xi - r_1^2)[A_1\cos(r_1 x) + A_2\sin(r_1 x)]\\
&\quad + (\xi - r_2^2)[A_3\cos(r_2 x) + A_4\sin(r_2 x)]\Big\}\,,\\
u'_A(x) &= -\, r_1 A_1\sin(r_1 x) + r_1 A_2\cos(r_1 x)\\
&\quad - r_2 A_3\sin(r_2 x) + r_2 A_4\cos(r_2 x)\,,\\
E_{zA} &= \frac{D_0}{\varepsilon_{33}^{A*}} - \frac{e_{31}^{A*}}{\varepsilon_{33}^{A*}}u'_A - \frac{p_3^{A*}}{\varepsilon_{33}^{A*}}T\,.
\end{aligned}
\tag{6}
$$

Here, the integration constants are:

$$A_1 = \frac{[b - a(k - \xi + r_2^2)][1 - \cos(r_1 l)]}{r_1(r_1^2 - r_2^2)\sin(r_1 l)}\,, \qquad A_2 = -\frac{[b - a(k - \xi + r_2^2)]}{r_1(r_1^2 - r_2^2)}\,,$$
$$A_3 = \frac{[b - a(k - \xi + r_1^2)][\cos(r_2 l) - 1]}{r_2(r_1^2 - r_2^2)\sin(r_2 l)}\,, \qquad A_4 = \frac{[b - a(k - \xi + r_1^2)]}{r_2(r_1^2 - r_2^2)}\,.$$

To find the elastic-brittle debond length of the possible delamination along the interface of the patch/layer structure the following criterion is used:

$$\tau_I(x) = \tau^{\mathrm{cr}}\,. \tag{7}$$

where τ^{cr} is the critical value of the interface stress for the adhesive. The value of x in the overlap zone $0 < x < l$, for which Eq. (7) is satisfied, is the *debond length* or *delamination length*. Graphically, it is the intersection of the interface shear stress as a function of x and the value of τ^{cr} for a given adhesive.

For the reasons of safe operation of the structure it is important to find the resonant frequency, which is dangerous for the structure's stability. These resonant frequency can occur if the displacements become too large, i.e., the denominators in the integration constants A_i, $i = 1 \div 4$ go to zero. Hence, for constants A_i at CASE 2 it results to condition $r_1^2 + r_2^2 \to 0$, or after some transformations and rearrangement, to the next quadratic equation about the resonant frequency:

$$\omega^2 = \frac{G_I}{h_I}\Big(\frac{E_A h_A + E_B h_B}{h_A h_B(\rho_A h_A + \rho_B h_B)}\Big)\,. \tag{8}$$

It has to be notified that BB has to be positive to assure the existence of 2 roots (positive and negative) for CASE 2.

Respectively, for constants A_i at CASE 3, the condition is different $r_1^2 - r_2^2 \to 0$, and leads to the following bi-quadratic equation in respect to the resonant frequency:

$$P\omega^4 + Q\omega^2 + R = 0\,, \tag{9}$$

where the values of coefficients P, Q and R are

$$P = \Big(\frac{\rho_A}{E_A} - \frac{\rho_B}{E_B}\Big)^2$$
$$Q = \frac{2G_I(\rho_A E_B - \rho_B E_A)(h_A E_A - h_B E_B)}{h_I h_A h_B (E_A E_B)^2}\,,$$
$$R = \frac{G_I(h_A E_A + h_B E_B)}{h_I h_A h_B E_A E_B}\,.$$

For CASE 3, the requirments for existing of two negative roots for z are AA and BB to be negative, and $AA^2 + 4BB$ to be positive or zero.

As it is seen, the resonant frequency will depend on the patch/layer materials 'densities and Young moduli, their thicknesses and on the shear modulus of the adhesive used in the construction. An example of the full frequency analysis for similar kind of problem (interface behavior of bi-material plate under time-harmonic load) could be found in our previous paper [26]. In the next section, the behavior of the considered structure described by the model represented will be illustrated with real data for the patch/layer structure, the adhesive, the geometry and the given combined load.

4 Numerical Examples

In order to illustrate the abovementioned results on the behavior of the interface shear stress, electric field and appearance of a possible interface delamination, the following materials $BaTiO_3$/Unreinforced epoxy (Table 1) and three type of adhesives (Ta-

Table 1: Materials' properties of the patch and host layer

Material and physical constants		Layer A $BaTiO_3$	Ref.	Layer B Unreinforced epoxy	Ref.
Elastic stiffness constants, GPa	c_{11}	150	[20]	3.5	[21]
	$c_{12} = c_{21}$	66		0	
	$c_{23} = c_{32}$	66		0	
	$c_{13} = c_{31}$	66		0	
	c_{22}	150		0	
	c_{33}	146		0	
Piezoelectric constants, C/m^2	$e_{31} = e_{13} = e_{32} = e_{23}$	- 4.35	[20]	0	[21]
	e_{33}	17.5		0	
Dielectric constants, $\times 10^{-10}$ C/(V m)	ε_{11}	98.7	[20]	0	[21]
	ε_{33}	111.6		0	
Pyroelectric constants, $\times 10^{-6}$ C/(K m^2)	p_3	20	[22]	0	[21]
Thermal stress coefficients, $\times 10^6$ N/(K m^2)	α_{11}	0.09329	[20]	0.21	[21]
	α_{22}	0.09329		0.21	
	α_{33}	0.09329		0.21	
Moisture stress coefficients, $\times 10^6$ N/(K m^2%)	β_{11}	0	[20]	7	[21]
	β_{22}	0		7	
Density, $\times 10^3$ (kg/m^3)	ρ	5.7	[20]	2.7	[21]

Table 2: The properties of adhesives

Adhesives	E, elastic modulus, GPa	ν, Poisson ratio	G_I, shear modulus, MPa	τ^{cr}, ultimate shear strength, MPa	Ref.
Thermoplastic polyacrylate glue (TPA)	2.5	0.5	800	18	[15, 23]
Araldite®2011 (AW 106/HV 953U)	1.35	0.45	465	33	[23, 24]
Araldite AV 119	3	0.35	1110	70	[9, 25]

ble 2) are chosen. The other parameters (geometric, electric, temperature, moisture concentration parameters) of the structure are constant as: $l = 0.08$ m, $T = 300$K, $H = 0.25\%$, $D_0 = 2.55$ C/m^2, unless otherwise stated.

The considered patch/layer structures have been investigated at different thicknesses of the adherends: $h_A = 0.001$ m, $h_B = 0.01$ m and $h_A = 0.01$ m, $h_B = 0.1$ m. The thinner structure corresponds to solution (CASE 2), with one positive and one negative root, Eqs. (5), while the thicker structure corresponds to solution (CASE 3) with two negative roots, Eqs. (6). The values of the resonant frequencies are calculated from Eq. (8) and Eq. (9) for both Cases and for the chosen materials, adhesives and thicknesses (Table 3). For CASE 3 and all adhesives considered, the discriminant in Eq. (9) is negative, or no real resonant frequencies exist.

Table 3: Resonant frequencies for both solutions at different adhesives

	Type of adhesive		
	TPA	AW 106/HV 953U	AV 119
CASE 2: $h_A = 0.001$ m, $h_B = 0.01$ m	56.2685	42.899	66.279
CASE 3: $h_A = 0.01$ m, $h_B = 0.1$ m	N/A	N/A	N/A

The shear stress, electric gradient and debond length in the patch/layer structure are calculated by both model solutions (CASE 2 and CASE 3) and the influence of the adhesive type, applied mechanical load σ_0, frequency ω, and electric displacement is investigated. All calculations are performed on Mathcad Prime, all graphics are created with Sigma Plot, v.13. It has been found that the influence of the temperature and humidity is not significant and their values remain constant. The influence of the geometry i.e., the change in the adherends‘ thickness is taken into account in the different types of solutions.

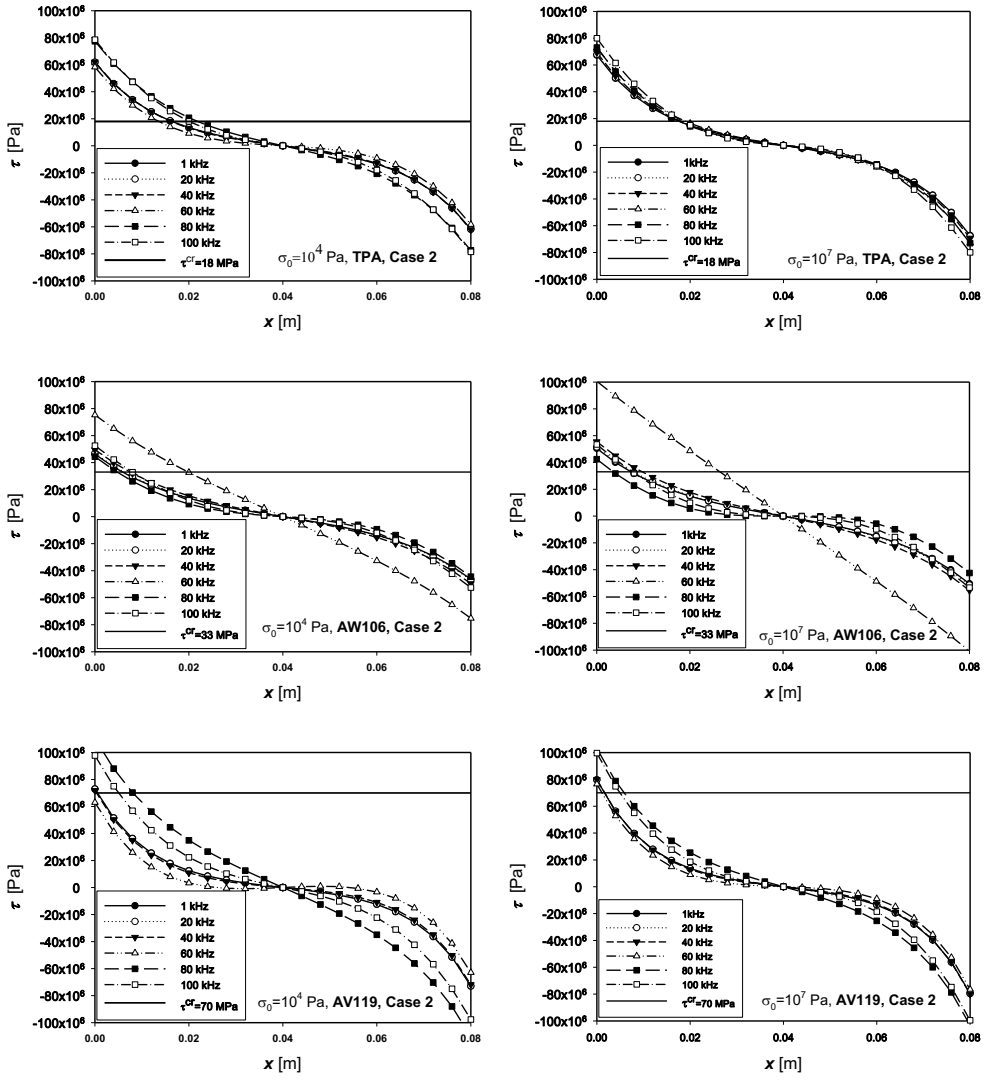

Fig. 2: Interface shear stress as a function of x for 3 different adhesives, at different σ_0 and ω – CASE 2.

The influence of the adhesive's type on the values of the interface shear stress for both solutions – CASE 2 and CASE 3, is presented in Fig. 2 and Fig. 3, respectively. It can be seen, that each adhesive has a different value τ^{cr} of the critical interface stress. In both figures, the interface shear stress and the possible delamination (intersection of $\tau_I(x)$ and τ^{cr}) in the overlap zone depend on both this level and the values of

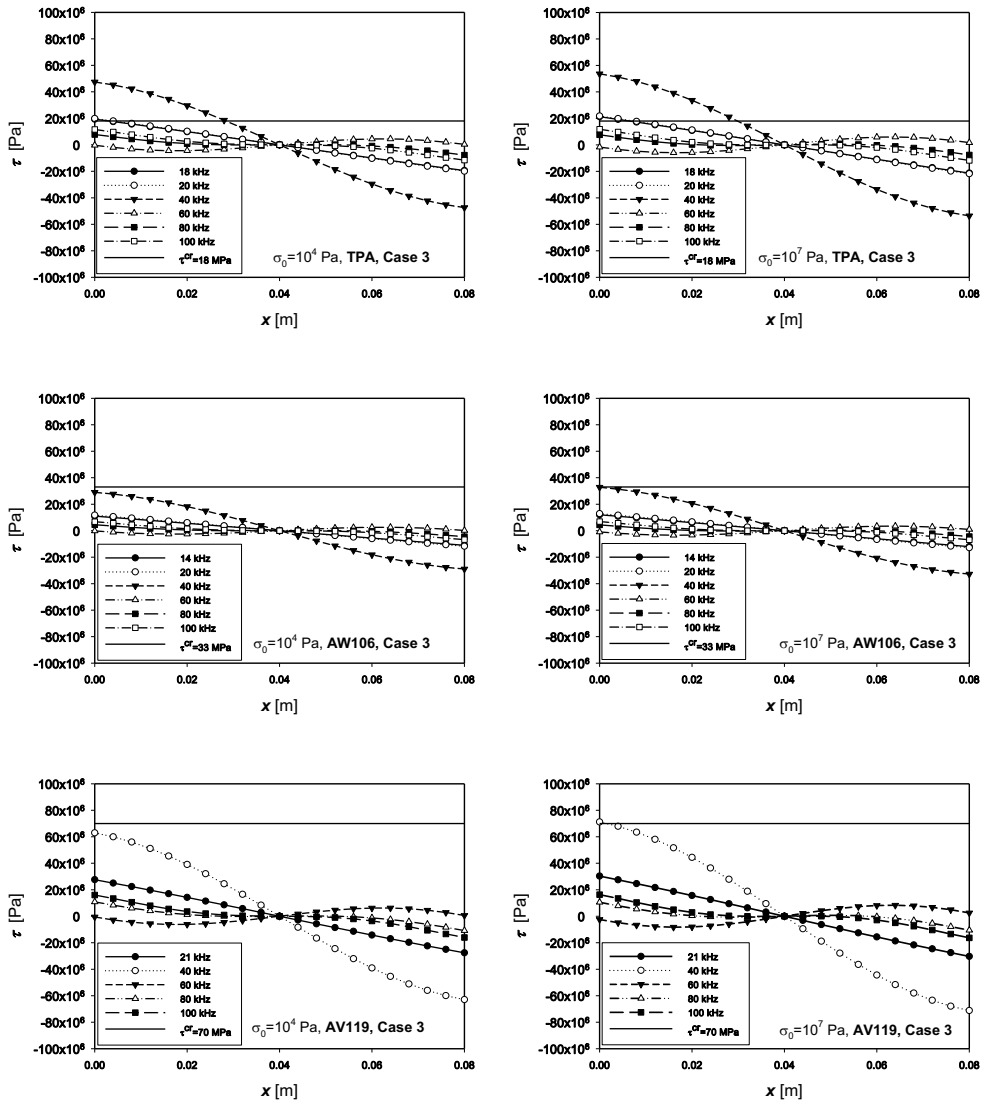

Fig. 3: Interface shear stresses as a function of x for 3 different adhesives, at different σ_0 and ω – CASE 3.

applied mechanical load. A weaker influence of the frequency values on the interface shear stress is seen for CASE 2; for CASE 3 (Fig. 3), this influence is better visible.

For CASE 2, (weakest adhesive TPA) the frequency of applied loading does not affect the interface shear stress. The latter remains practically unchanged, especially

in case of higher mechanical loading. For adhesive AW 106, the behavior is the same, except the case of the highest frequency corresponding to the highest delamination value, and it increases with an increase of the mechanical load value. For the strongest adhesive AV 119 the delamination depends on the values of the frequency and it is better "separated" for low mechanical load, than higher one. As expected, delamination is the highest one for the weakest adhesive, but it should be mentioned that no parameter can affect its value. For the other two adhesives by changing the magnitude and frequency of the applied loadings, it can be expected that the delamination should be only minimal, which is desirable for the safe operation of many electronic devices and sensors.

For CASE 3 (Fig. 3) the behavior of the interface shear stress for the three adhesives is totally different – practically there is no delamination for AW 106 and AV 119 in the investigated intervals of loadings and frequencies. Only for the weakest adhesive, delamination occurs and this happens for the frequency about 40 kHz, and higher loading.

One additional validation that results obtained for $\tau_I(x)$ are in the "safe" frequencies range is the fact, that the dangerous resonance frequencies for both CASE 2 and CASE 3 (Table 3) are outside the range of the frequencies studied (see Fig. 2 and Fig. 3). As it has been reported in [19], for PZT-5H/CFRP, both solutions (CASE 2 and CASE 3) are obtained and change from one to another at constant thicknesses of patch/layer and exactly determined frequency (limit frequency, after which the solution changes). The debond lengths for CASE 2 and CASE 3, for all adhesives considered, as functions of mechanical loadings ($10^4 \div 10^7$ Pa) and frequencies (1–60 kHz) are presented in Fig. 4. The behavior of the debond lengths confirms the results represented in the Fig. 2 and Fig. 3 for the interface shear stress. For simplicity, the legend with the mechanical loadings is the same for all results represented in Fig. 4.

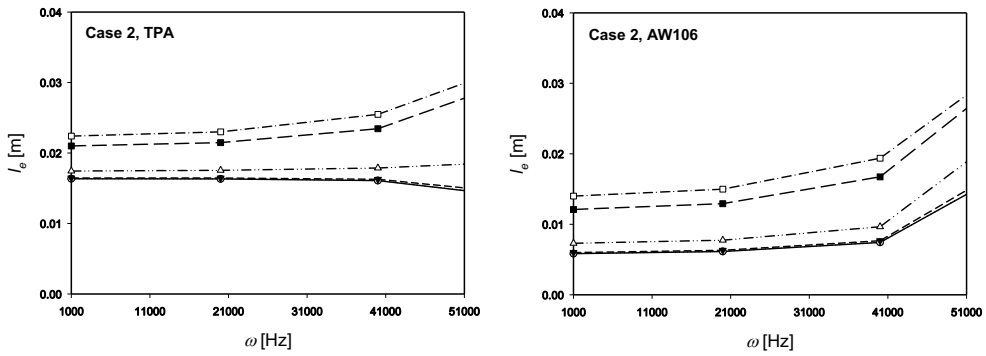

Fig. 4: Behavior of the debond lengths for CASE 2 and CASE 3.

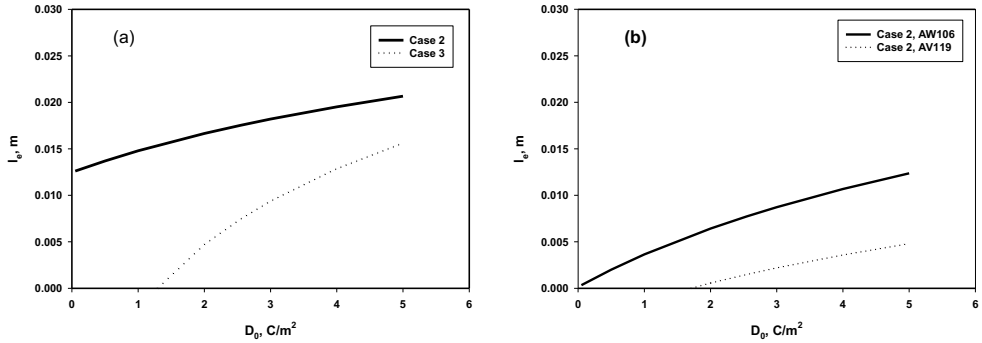

Fig. 5: Influence of D_0 on the debond length for $\sigma_0 = 10$ MPa and $\omega = 20$ kHz; (a) for CASE 2 and CASE 3, adhesive TPA and (b) for CASE 2 only, adhesives AW106 and AV119.

For CASE 2, the delamination length increases with increasing the magnitude and frequency of the applied mechanical loading, for the first two adhesives, reaching 0.035m (about 40% of overlap zone). For AV 119 the delamination reaches a maximal value of 0.015 m (about 18% of the overlap zone), for the highest magnitude and frequency of the applied mechanical loading. On a contrary, for CASE 3, there is a delamination only for the first adhesive, which increases with increasing the magnitude and frequency of the applied mechanical loading. Also, delamination appears between 18–38 kHz for the first adhesive, there is no delamination for this adhesive outside this interval.

The influence of electric displacement D_0 on the debond length (all other parameters are constant) is shown for adhesive TPA in the Fig. 5(a). It is seen, that if the other parameters are constant, the "safe" values of D_0 for CASE 3 (without delamination) are less than 1.5, after that value the debond length increases with increasing D_0. For CASE 2 there are no "safe" values of D_0, the debond length increases with increasing D_0, as the values of l_e are larger than those for CASE 3. For the other two adhesives only CASE 2 gives non zero debond lengths as the influence of D_0 is presented in the Fig. 5(b). In this case only adhesive AV 119 has a "safe" interval of D_0 from 0 to 1.5 with no delamination.

The behavior of the electric gradient in the overlap zone for the adhesive TPA, in CASE 2 and CASE 3 is represented in Fig. 6. For the other two adhesives, the behavior of the electric gradient is absolutely the same. In practice, the electric gradient changes along the length of the overlap zone, at constant magnitude and frequency of the applied mechanical loading (see the embedded graphics), but in the large range of the ordinate axis it looks like a straight line. The electric gradient increases with increasing the value of electric displacement for all adhesives, in both Cases.

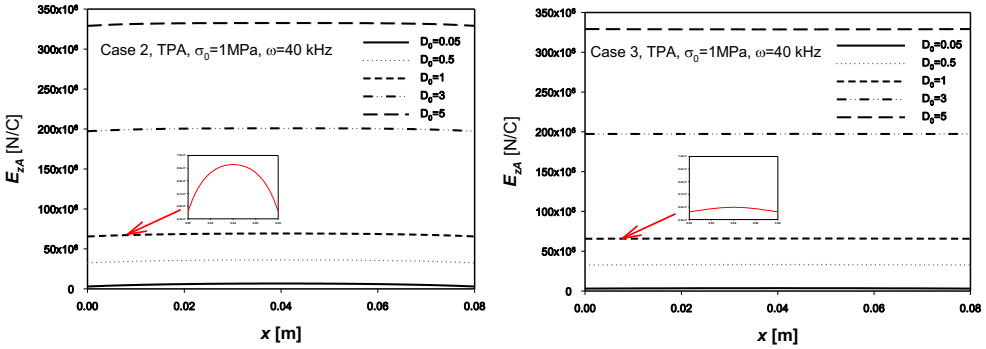

Fig. 6: Behavior of the electric gradient as a function of x, CASE 2 and CASE 3.

The future plans of the authors will include the investigation of the another combinations of materials for the structure layers and adhesives, as well as the influence of the overlap length of the structure on the delamination in it. The proposed method of solution gives the possibility to predict fast and analytically the safe intervals for the healthy work of adhesively bonded bi-material structures under quasi-static time harmonic load at environmental conditions and in the presence of electric field.

5 Conclusions

The interface debonding of an adhesively bonded piezoelectric patch on a host layer structure subjected to quasi-static time harmonic mechanical loading and electric field at environmental conditions has been studied. The closed form solutions for the interface shear stress and debond length have been applied and discussed. The influence of the adhesive type on the interface debond length at two types of solutions for (CASE 2 and CASE 3) has been presented and illustrated on $BaTiO_3$/epoxy patch/layer structure, at three types of adhesives.

The combined load (mechanical in the presence of electric field) strongly influences the values of the interface shear stress and debonds length, for all adhesives. The influence of the temperature and humidity is not significant. A stronger adhesive leads to a reduced interface delamination.

For all adhesives, the frequency influence on interface shear stress and debond length can be seen more clearly for thicker layer's structure (CASE 3), than thinner one (CASE 2). The electric gradient is slightly affected by the magnitude and frequency of the applied mechanical loading, and it is highly dependent on the magnitude of electric displacement. In addition, for the reasons of safe operation of the patch/layer structure, the analytical equations for resonant frequencies for both solutions at all three investigated adhesives are developed for the first time and they are

calculated for both type of solutions, where it is possible. They should be used for the fast prediction of resonant frequencies in similar kind of structures and loads.

ACKNOWLEDGEMENTS

This research did not receive any specific grant from funding agencies in the public, commercial, or not-for-profit sectors.

REFERENCES

[1] S. BUDHE, M.D. BANEA, S.DE BARROSA, L.F.M. DA SILVA (2017) An updated review of adhesively bonded joints in composite materials. *International Journal of Adhesion and Adhesives* **72** 30-42.

[2] KWANG-SOO KIM, JAE-SEOK YOO, YEONG-MOO YI, CHUN-GON KIM (2006) Failure mode and strength of uni-directional composite single lap bonded joints with different bonding methods. *Composite Structures* **72** 477-485.

[3] M. KASHFUDDOJA, M. RAMJI (2014) Critical analysis of adhesive layer behavior in patch-repaired carbon fiber-reinforced polymer panel involving digital image correlation. *Journal of Composite Materials* **49**(16).

[4] C. JIN, X.D. WANG, M.J. ZUO (2010) The dynamic behaviour of surface-bonded piezoelectric actuators with debonded adhesive layers. *Acta Acta Mechanica* **211**(3) 215-235.

[5] L.F.M. DA SILVA, R.D.S.G. CAMPILHO (2011) "Advances in Numerical Modelling of Adhesive Joints". Springer Science & Business Media.

[6] X.-L. ZHAO, Y. BAI, R. AL-MAHAIDI, S. RIZKALLA (2014) Effect of dynamic loading and environmental conditions on the bond between CFRP and steel: State-of-the-art review. *Journal of Composites for Construction* **18**(3).

[7] Y. ZHU, K. KEDWARD (accessed 09.09.2021) Methods of analysis and failure predictions for adhesively bonded joints of uniform and variable bondline thickness, Final report. http://www.tc.faa.gov/its/worldpac/techrpt/ar05-12.pdf.

[8] H. MATT, I. BARTOLI, F.L. DI SCALEA (2005) Ultrasonic guided wave monitoring of composite wing skin-to-spar bonded joints in aerospace structures. *The Journal of the Acoustical Society of America* **118**(4) 2240-2252.

[9] M. SANDU, A. SANDU, D.M. CONSTANTINESCU (2010) Strength of adhesively bonded single-strapped joints loaded in tension. In: *Proceedings of the Romanian academy*. The Publishing House of the Romanian Academy, Series A **11**(4) 371-379.

[10] H.A. TINOCO, A.L. SERPA, A.M. RAMOS (2010) Numerical study of the effects of bonding layer properties on electrical signatures of piezoelectric sensors. *Mecánica Computacional* **XXIX** (artículo completo). E. Dvorkin, M. Goldschmit, M. Storti (Eds.), Buenos Aires, Argentina, 15-18 Nov. 2010, pp. 8391-8409.

[11] M. AFENDI, R. DAUD, I.H.B.W. NORDIN, T. TERAMOTO (2012) Strength and fracture characteristics of shear adhesive dissimilar joint. In: *Proceedings of International Conference on Applications and Design in Mechanical Engineering (ICADME 2012)*, 27^{th} - 28^{th} February 2012, Penang, Malaysia, 2012.

[12] R.D.S.G. CAMPILHO (2009) Repair of composite and wood structures. Faculty of Engineering of Porto University, Department of Mechanical Engineering and Industrial Management, PhD Thesis.

[13] S.M. KASHIF (2012) Delamination effect modeling, simulation and experimental validation of lap shear test. *International Journal of Mechanical and Materials Engineering (IJMME)* **7**(3) 177-185; Corpus ID: 73570290.

[14] A. CHADEGANI, R.C. BATRA (2011) Analysis of adhesive-bonded single-lap joint with an interfacial crack and a void. *International Journal of Adhesion and Adhesives* **31** 455-465.

[15] V. VALEVA, J. IVANOVA, B. GAMBIN (2011) BEM and shear lag method for interface problem of bi-material structure under static loading. *Journal of Theoretical and Applied Mechanics* **49**(1) 17-29.

[16] C. JIN, X. WANG (2011) The Effect of adhesive layers on the dynamic behavior of surface-bonded piezoelectric sensors with debonding. *Journal of Intelligent Material Systems and Structures* **22**(7).

[17] P. HASS, F.K. WITTEL, P. NIEMZ (2013) Generic failure mechanisms in adhesive bonds. *Holzforschung* **67**(2) 207-215.

[18] T.A.B. FERNANDES, R.D.S.G. CAMPILHO, M.D. BANEA, L.F.M. DA SILVA (2015) Adhesive Selection for Single Lap Bonded Joints: Experimentation and Advanced Techniques for Strength Prediction. *The Journal of Adhesion* **91** 841-862.

[19] E. KIRILOVA, T. PETROVA, W. BECKER, J. IVANOVA (2017) Influence of the geometry and the frequency range on the interface delamination in smart patch/layer structures under combined dynamic loading. *ZAMM - Journal of Applied Mathematics and Mechanics / Zeitschrift fr Angewandte Mathematik und Mechanik* **97**(9) 1136-1146.

[20] Y. HE (2004) Heat capacity, thermal conductivity, and thermal expansion of barium titanate-based ceramics. *Thermochimica Acta* **419** 135-141.

[21] R.S.C. KURAVI (2011) "Controlling deformation in elastic and viscoelastic beams due to temperature and moisture changes using piezoelectric actuator". Master's thesis, Texas A&M University.

[22] D.D.L. CHUNG (2010) "Functional Materials: Electrical, Dielectric, Electromagnetic, Optical and Magnetic Applications". World Scientific Publishing Co Pte Ltd, Singapore.

[23] J. LEMAITRE, R. DESMORAT, M.R. VIDONNE, R. ZHANG (1996) Reinitiation of a crack reaching an interface. https://doi.org/10.1007/BF00018507*International Journal of Fracture* **80** 257-276.

[24] M. SANDU, A. SANDU, D.M. CONSTANTINESCU, Ş. SOROHAN, D.A. APOSTOL (2013) Performance of sandwich components with chiral topology cores. In: *Proc. of 13th Intern. Conference on Fracture*, 16^{th} – 21^{st} June 2013, Beijing, China, pp. 1-10.

[25] W.R. BROUGHTON, R.D. MERA (1999) Environmental degradation of adhesive joints, accelerated testing. *NPL Report CMMT(A) 197*.

[26] J. IVANOVA, G. NIKOLOVA, P. DINEVA, W. BECKER (2010) Interface behavior of bimaterial plate under time-harmonic load. *Journal of Mechanical Engineering* **136**(10) 1194-1201.